THE ASTROPHYSICAL JOURNAL, 401:L11–L14, 1992 December 10

BROAD BAND X-RAY TELESCOPE OBSERVATIONS OF NGC 4151: IRON LINE DIAGNOSTICS

K. A. WEAVER,[1] R. F. MUSHOTZKY, K. A. ARNAUD,[1] P. J. SERLEMITSOS, F. E. MARSHALL,
R. PETRE, K. M. JAHODA, E. A. BOLDT, S. S. HOLT, J. SWANK, A. E. SZYMKOWIAK,
R. KELLEY, A. P. SMALE,[2] AND C. DONE[3]
NASA/Goddard Space Flight Center, Greenbelt, MD 20771
Received 1992 August 5; accepted 1992 September 24

ABSTRACT

The Fe Kα emission line is a potentially powerful diagnostic tool in the X-ray spectra of AGNs, however, this feature has previously been observed with relatively poor spectral resolution. The Broad Band X-Ray Telescope (BBXRT) has provided us with the first high-quality, medium-resolution X-ray spectral data. We are able to constrain the width of the 6.4 keV Fe Kα line in NGC 4151 to be less than 160 eV FWHM (7,500 km s^{-1}), in contrast with former measurements of the line width. Also, we have limited information on the shape of the line profile. In addition to the strong narrow Fe Kα feature, we detect weaker broad residuals between 5–8 keV.

Subject headings: galaxies: individual (NGC 4151) — galaxies: nuclei — galaxies: Seyfert

1. INTRODUCTION

NGC 4151 is one of the best studied Seyfert 1 galaxies at X-ray wavelengths (Yaqoob & Warwick 1991, and references therein). It is also one of the intrinsically weakest Seyferts, having an observed $L_{X(2-10)} \sim 7 \times 10^{42}$ ergs s^{-1}. X-ray continuum variability time scales of order days have been seen as well as marginal evidence for a flux-index correlation (Yaqoob & Warwick 1991, hereafter YW91). NGC 4151 has a fairly complex continuum shape which has previously been measured by instruments on *HEAO 1*, *Einstein*, *EXOSAT* and *Ginga*. The 2–10 keV spectrum consists of an absorbed power law with a variable photon index, ranging from 1.35–1.7 (YW91). Below ~4 keV, there is a soft X-ray excess above absorption by a uniform intrinsic absorber, which has been interpreted as partial covering of the central source (Holt et al. 1980). The measured column density is $\sim 10^{23}$ cm^{-2} and appears to be variable on time scales of months to years (Yaqoob, Warwick, & Pounds 1989). NGC 4151 has an unusually strong 6.4 keV Fe Kα emission feature, with a possibly variable equivalent width (YW91). The high equivalent width (~160 eV) has previously been explained in terms of geometrical effects, possible time lag effects (Makishima 1986) and/or a high Fe abundance. To date, the intrinsic line width has not been measured due to the poor spectral resolution of proportional counters (~20% at 6 keV). BBXRT, with ~3% resolution at 6.0 keV offers the first opportunity to directly measure the width of the Fe Kα line.

2. INSTRUMENT DESCRIPTION

The Broad Band X-ray Telescope, which flew successfully on the Space Shuttle *Columbia* as part of the *Astro-1* mission in 1990 December, consists of two identical telescopes with lightweight nested foil mirrors to focus X-rays onto two segmented (five elements, hereafter referred to as pixels) solid state detectors. This design allows for crude spatial resolution for diffuse sources as well as improved background discrimination. The radius of the central pixels (designated A0 or B0) is 2′, and the total diameter of the outer 4 pixels (A–B; 1–4) is 17′. The bandpass of BBXRT is 0.3–12 keV, which offers improvement over proportional counters and previous solid-state detectors in that both the soft and medium X-ray regimes are covered simultaneously. A full discussion of the instrument and calibration can be found in Serlemitsos et al. (1991) and Weaver (1993).

Observations of the on-board Fe^{55} calibration source were made throughout the mission. The final energy scale was determined by a quadratic fit to the in-flight calibration data as well as some lower energy atmospheric lines: argon and oxygen fluorescence as well as Si XIII and Mg XI from scattered solar X-rays. We were able to view the Crab nebula, a standard X-ray calibration source, five times: both centered and offset by ~4′. The effective area curves for the 10 BBXRT pixels were refined based on fitting the Crab spectrum as well as other bright sources (Weaver 1993). Between 3–7.5 keV, the residuals to the Crab are no more than 5%, while some residuals still remain at the 10% level for energies greater than 7.5 keV (Fig. 1).

Since the spectrum of NGC 4151 is known to be complex at low energies we restrict ourselves to data above 2 keV in this analysis. The low internal detector background at high energies is found to scale with the detector guard rate, a housekeeping parameter indicating the rate of particle interactions with the plastic scintillator surrounding most of the detector (Jahoda et al. 1993). The external background at energies greater than 2 keV is approximately constant provided we were not observing during a solar flare. In order to perform a proper background subtraction, night background data was accumulated and then renormalized to the guard rate for each source observation and subtracted. Since the 2–10 keV background count rate (~0.01–0.04 counts s^{-1} $pixel^{-1}$) is much smaller than the source count rate (1.2–2.2 counts s^{-1} $pixel^{-1}$), this simple one step method is very reliable.

Pointing inaccuracies present the largest problem for the data analysis due to the effects of energy-dependent vignetting at higher energies as a function of off-axis position. A log of BBXRT observations of NGC 4151 is listed in Table 1. The total time spent on source was 6116 s and was divided among six observations. Two pointings placed the source in the

[1] Also University of Maryland.
[2] With the Universities Space Research Association.
[3] NAS/NRC Resident Research Associate.

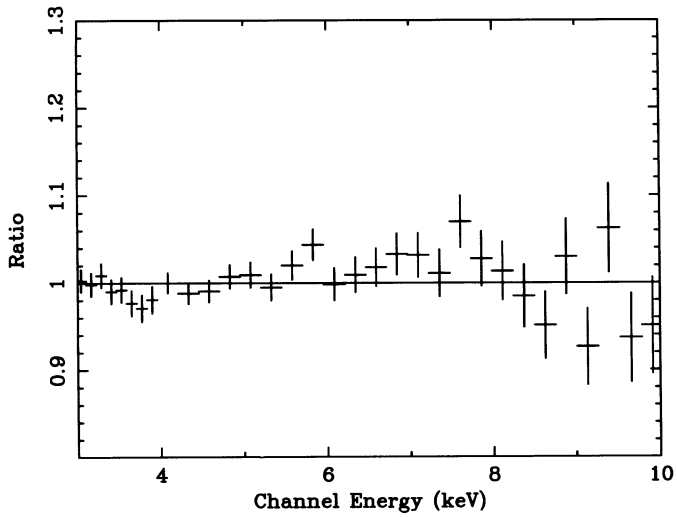

FIG. 1.—Plot of the 3–10 keV residuals of the Crab data to the best-fit model ($N_H = 0.3 \times 10^{22}$ cm^{-2}, $\Gamma = 2.1$) using the 1992 June 1 response matrix. The data are binned so that each bin is about 250 eV wide (on the order of twice the energy resolution of the instrument).

central pixels. The other four are located in sets of outer pixels, between 5′–9′ off-axis. The exact position of the source in detector coordinates is not known as aspect camera data, allowing the matching of stars in the field, are not available for the NGC 4151 pointings. However from the ratios of count rates in all detector elements along with knowledge of the mirror point response function, we are able to obtain fairly accurate off-axis positions. The uncertainty in each estimate is $\sim$1′–2′.

3. RESULTS

The 2–10 keV data were fit with a partially covered power law continuum [the photon index Γ is defined as $N(E) \propto E^{-\Gamma}$] and a narrow Gaussian. Multiple pulse-height data files extracted for a specific pixel during a given time range were fit simultaneously using the XSPEC spectral fitting package (Shafer et al. 1989) with appropriate detector response matrices. In order to use chi-square statistics, the data were binned to have a minimum of 20 counts per bin. For each observation listed in Table 2, the A and B pixel data were fit together. Observations 1 and 2 represent fits utilizing two data files. Observations 3 and 4, being closely spaced in time, were fit simultaneously as were observations 5 and 6 (four data files each). The observed values of $\Gamma \sim 1.65$ and $N_H \sim 7 \times 10^{22}$ cm^{-2} listed in Table 2 are consistent with previous observations for NGC 4151. Fitting the 2–10 keV data alone do not constrain either parameter well enough to test for variability. The observed covering fraction of $\sim$91% is also typical for this source (Holt et al. 1980).

TABLE 1

LOG OF BBXRT OBSERVATIONS OF NGC 4151

Observation	MET[a] (decimal day)	Duration (s)	Pixel	Off-Axis	Total 2–10 keV Count Rate (counts s^{-1})
1	3.833	897.9	A3/B1	5.5	4.66 ± 0.12
2	5.618	691.2	A3/B1	6.0	4.08 ± 0.22
3	5.906	1079.1	A2/B4	4.0	5.60 ± 0.12
4	5.927	1150.2	A0/B0	0.0	5.53 ± 0.10
5	6.605	747.7	A2/B4	4.5	3.50 ± 0.08
6	6.622	1555.2	A0/B0	1.5	3.57 ± 0.06

[a] 0^h MET is 1990 day 336 $06^h49^m01^s$ UT.

One of our primary goals is measuring the profile of the Fe Kα emission feature at $\sim$6.4 keV which is thought to arise due to reprocessing of the X-ray continuum by fluorescence of iron in a cold ($T \leq 10^5$ K) gas (Lightman & White 1988). Fitting a Gaussian to the BBXRT data gives a $\Delta\chi^2$ of 40 which is significant at $\gg$99% confidence. The major component of the Fe Kα line measured with the best signal-to-noise (S/N) observation, is narrow, with a 90% confidence upper limit of 160 eV (7500 km s^{-1}) FWHM. This is in strong contrast with a FWHM of $\sim$38,000 km s^{-1} previously seen in this object (YW91). The measured line peak energy of 6.35 ± 0.03 is consistent with redshifted cold iron ($z = 0.003$) at 90% confidence, and the ionization state is restricted to be less than Fe XIII. The maximum allowed energy shift for cold iron is 0.070 keV (3300 km s^{-1}).

An important discriminator between different theories for the origin of the Fe Kα line is its variability. We observed the 2–10 keV source flux increase by $\sim$40% in 8 hours and similarly decrease over a period of 17 hours (Fig. 2*a*). Only the last two observations had sufficient S/N to test the variability of the Fe Kα line. During this time, the line flux remains constant at a value of 0.0003 photons s^{-1} (Fig. 2*b*), while there is a weak trend (more than 75% confidence) for the equivalent width (EW) to increase from $\sim$90 eV to $\sim$170 eV (Fig. 2*c*). The one-dimensional error contours are shown in Figure 3 (*insert*) which also illustrates the best fit to the Fe Kα line using the summed central pixel data only.

Next, we investigated the Fe K-edge, utilizing the highest S/N observations (Nos. 3–6). The days 5 and 6 A0 and B0 data were added together and fit simultaneously with the summed A2 and B4 data. To determine the edge energy the data were fit from 3–10 keV with an absorbed power law and Gaussian, but setting the Fe abundance to zero. First an edge was added with an optical depth $\tau = 0.1$, corresponding to solar Fe abundance as compared to the low-energy absorbing column $N_H \sim 7 \times 10^{22}$ cm^{-2}. This gives an edge energy of 7.46 ± 0.23 keV (90% confidence) and a $\Delta\chi^2$ of 12 which is significant at greater than 99% as measured by an *F*-test. The lowest allowed energy, 7.23 keV, is slightly higher than an edge for neutral iron of 7.1 keV and represents an ionization state of Fe V–XVIII (Makishima 1986).

After including a solar Fe K-edge, a feature remains in the data at the 10% level appearing as an excess of counts surrounding Fe Kα (Fig. 4). The observed excess can be partially modeled by allowing the edge optical depth to be free which gives $\tau = 0.28 \pm 0.1$ (90% confidence) and a $\Delta\chi^2$ of 8, which is significant at greater than 99% confidence for the addition of one free parameter. This corresponds to a factor of 2.8 ± 1.0 in the abundance of iron, which is in agreement with previous overabundance measurements (Holt et al. 1980; YW91). A better fit results from adding a broad Gaussian with a FWHM of $\sim$1.6 keV centered at 6.1 ± 0.6 keV (90% errors obtained by fixing the line width at 1.6 keV) and an EW of $\sim$130 eV. In this case, $\Delta\chi^2 = 15$ which is significant at greater than 99% for the addition of three free parameters. Fitting a broad Gaussian and allowing the Fe K-edge depth to vary at the same time gives no improvement in the fit.

4. DISCUSSION

Line shape and variability (Kunieda et al. 1990) are crucial for determining the physical site for the origin of the Fe Kα line in Seyfert 1 galaxies. If much of the line is due to fluorescence of material in an accretion disk, its profile will be dominated by emission from the inner region of the disk (Fabian et al. 1989;

TABLE 2A

2–10 keV PARTIAL COVERING + Fe Kα FITS TO NGC 4151

Observation	Γ	90% Error	N_H (10^{22} cm^{-2})	90% Error	f_c	90% Error	F_{2-10} (ergs cm^{-2} s^{-1})	χ^2/ν
1	1.61	1.42–1.80	6.40	4.84–7.53	0.96	0.93–1.00	2.4E-10	124/141
2	1.68	1.28–1.94	8.16	5.02–11.2	0.90	0.85–0.94	1.2E-10	46/57
3 + 4	1.68	1.54–1.83	7.10	5.76–8.45	0.91	0.89–0.93	1.8E-10	337/367
5 + 6	1.59	1.43–1.74	8.49	6.68–10.3	0.90	0.88–0.93	1.2E-10	210/227

TABLE 2B

Fe Kα NARROW LINE PARAMETERS

Observation	E (keV)	90% Error (keV)	Sigma[a] (keV)	EW (eV)	90% Error (eV)	Flux (photons cm^{-2} s^{-1})	90% Error (photons cm^{-2} s^{-1})
1	6.35	6.30–6.40	0.0–0.13	157	92–218	5.4E-04	(3.4–8.0)E-04
2	6.37	6.29–6.44	0.0–0.42	159	45–240	2.8E-04	(0.8–5.1)E-04
3 + 4	6.32	6.28–6.37	0.0–0.17	88	60–128	3.0E-04	(1.6–3.6)E-04
5 + 6	6.35	6.32–6.38	0.0–0.07	165	112–211	3.0E-04	(1.5–4.5)E-04

[a] Represents measurements of the 90% confidence upper limit on the line width, which was frozen at 0.0 for the fit values in this table.

Laor 1991). We should therefore observe both general relativistic and Doppler effects. In particular, for low inclinations general relativistic effects dominate and the line is redshifted with a narrower profile. For higher inclinations the line is broadened and the mean energy is blueshifted.

Under the assumption that the Fe Kα line is produced in a disk, we initially fit a nonrotating disk line profile (Fabian et al. 1989) to measure how the line emissivity would vary as a function of disk radius. With the inner and outer radii fixed at $6r_g$ and $500r_g$ ($r_g = GM/c^2$), the measured peak line energy is found to be $E_{peak} = 6.43 \pm 0.05$ keV, the disk inclination is less than 30° (99% confidence), and the line emissivity varies as r^q, $q = -2.5$. We next used code supplied by A. Laor to search for relativistic effects on the line profile. Fixing the outer radius to be $500r_g$ and the line emissivity to vary as $r^{-2.5}$, we find the inner radius constrained to be greater than $20r_g$ and the inclination to be less than 15° (90% confidence). In both cases, adding a disk line reduces χ^2 by ~40, identical to adding a narrow Gaussian.

The face-on geometry required to produce the narrow Fe Kα feature is inconsistent with inferred geometries obtained by other methods. In particular, *Ginga* observations of NGC 4151 show little evidence for a component due to Compton reflection in an optically thick disk (Maisack & Yaqoob 1991). The fact that the contribution of reflection is minimal implies we are seeing the disk edge-on (George & Fabian 1991).

An alternative Fe Kα production site is the broad line region (BLR). We know there is a large amount of absorbing gas along the line of sight to the continuum source, as evidenced by the heavy absorption of soft X-rays (Holt et al. 1980). If the BLR is responsible for this absorption we should expect to observe an Fe Kα emission feature. We should also expect to see evidence of Keplerian dynamics $\delta E/E = \sigma_{Fe\,K}/c = (r_g/R_{BLR})^{1/2}$ where δE is the observed Gaussian width and $\sigma_{Fe\,K}$ is the FWHM in km s^{-1}. Maoz et al. (1991) find the emissivity weighted radius of the BLR in NGC 4151 to be ~17 light-days (4.4×10^{16} cm) which gives predicted values of $\sigma_{Fe\,K}$ from 2000 to 17,000 km s^{-1} for black hole masses ranging from

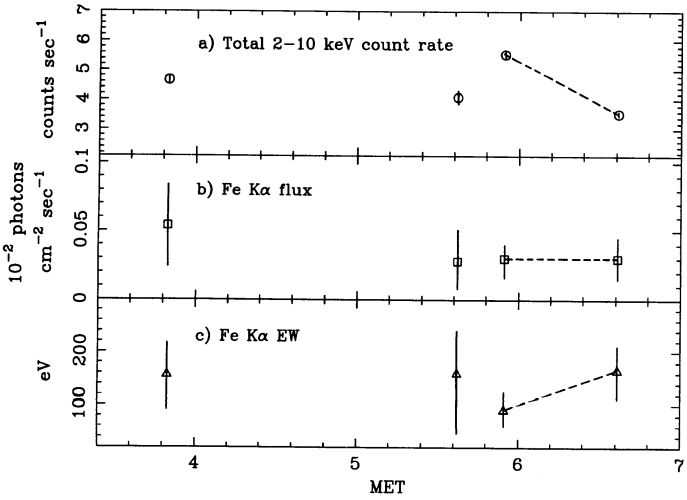

FIG. 2.—Variability of the continuum and Fe Kα line. (*a*) Total (vignetting corrected) source count rate for all detector elements added together. (*b*) Fe Kα line flux as a function of time throughout the mission. (*c*) Fe Kα equivalent width as a function of time. The dashed lines connect the highest S/N observations which are discussed in § 3.

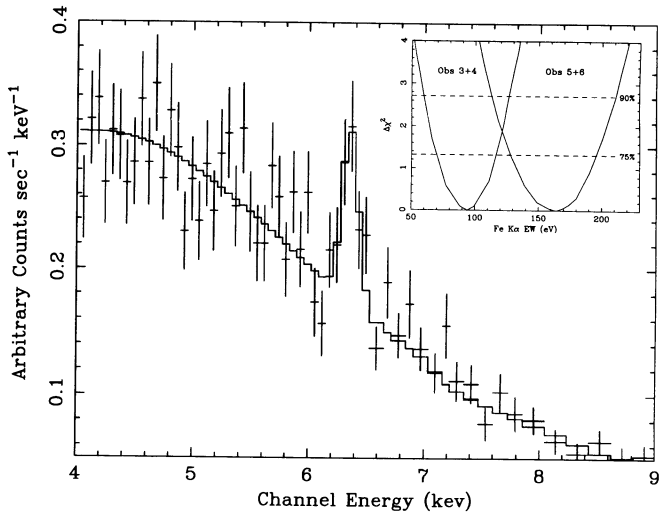

FIG. 3.—Illustration of the Fe Kα line profile using all the data from the central pixel elements. The solid histogram represents the best-fit model. Insert shows the one-dimensional error contours for the Fe Kα EW on day 5 MET (obs. 3–4) and day 6 MET (obs. 5–6).

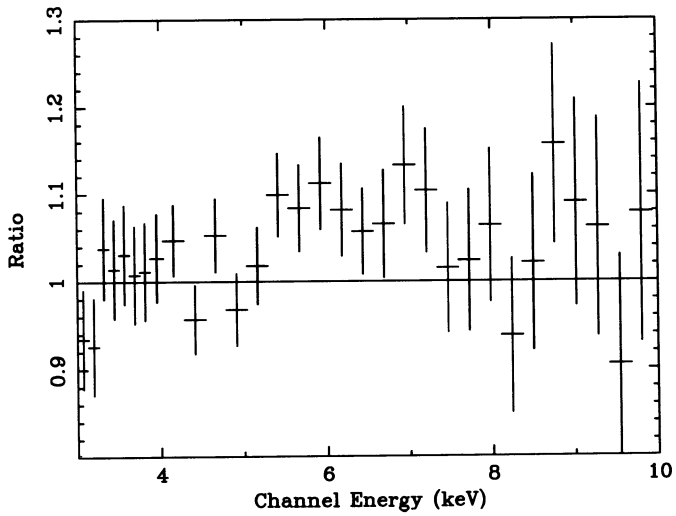

FIG. 4.—Illustration of residuals of the NGC 4151 data to the model which consists of an absorbed power law with the Fe abundance set to zero as well as a Gaussian and an additional Solar abundance Fe K edge. The data are binned in 250 eV wide bins.

10^7–10^9 $M_\odot$. Our result of $\sigma_{\mathrm{Fe\,K}} \leq 7500$ km s^{-1} falls within this range and is consistent with approximately simultaneous data for the broad C IV line obtained with the Hopkins Ultraviolet Telescope onboard the Space Shuttle *Columbia*, which had $\sigma_{\mathrm{C\,IV}} = 7600 \pm 500$ km s^{-1} (Kriss et al. 1992).

We can calculate the expected EW of the BLR Fe Kα line from (Halpern 1982):

$$\mathrm{EW} = 350\left(\frac{\Omega}{4\pi}\right)\left(\frac{N_{\mathrm{H}}}{10^{23}}\right)\left(\frac{A_{\mathrm{FE}}}{4\times10^{-5}}\right)\left(\frac{1}{\alpha+3}\right)\left(\frac{6.4}{7.1}\right)^{\alpha}\ \mathrm{eV}\ ,$$

where the spectral index $\alpha = \Gamma - 1$. For our observations ($\alpha \sim 0.6$, $N_{\mathrm{H}} \sim 10^{23}$) this gives 91 eV assuming full coverage and solar abundances. The 90% confidence lower limit on the measured Fe Kα EW for the first and last observations in Table 2 is slightly higher than this value. However, for the 2–3 times solar Fe implied by previous measurements of the Fe edge (Warwick et al. 1989; Holt et al. 1980) and allowed by our data, one can get an EW of greater than 250 eV. So, assuming a thick, spherical geometry for NGC 4151, the Fe Kα line is consistent with being produced in the BLR with a factor of 2 overabundance of Fe.

An additional argument for the Fe Kα line being produced far away from the central source is the lack of evidence for line flux variability. Since the line does not appear to track the continuum on a 17 hour time scale, it must originate at least 1.8×10^{15} cm away from the central source. If the line were produced in a disk which has $r_{\mathrm{in}} \sim 6r_g$ (1.3×10^{14} cm for a 10^8 $M_\odot$ black hole), it should have responded to the continuum in less than 4 hours.

To model the observed broad residuals, the data require either a 2–4 times overabundance of iron as measured with the K-edge or the addition of a broad Gaussian centered around 6.1 keV. The Fe K-edge in NGC 4151 has previously been seen to indicate a 2–3 times overabundance of iron, also consistent with the overabundance implied by the large EW of the narrow Fe K line. However, requiring a broad Fe Kα component would explain the discrepancy between the BBXRT narrow Fe Kα line and the Fe Kα line observed by *Ginga* (YW91) which was seen to have a FWHM of 38,000 km s^{-1}. In this scenario, the *Ginga* feature would be a convolution of a narrow and broad component with similar EWs as seen in the BBXRT data. The parameters we measure for the broad component are consistent with its being produced in an accretion disk (Matt et al. 1991). It may be the case that two Fe Kα lines are actually present in Seyfert 1 galaxies (one from the disk and one from the BLR) and the orientation and amount of intrinsic absorbing material in the galaxy will cause one line to dominate the other. Obtaining better S/N data with ASTRO-D should allow us to resolve this issue.

5. CONCLUSIONS

The major component of Fe Kα line is narrow (less than 7500 km s^{-1} FWHM) and its width is consistent with being produced in the broad line region.

An accretion disk line fit to the narrow Fe Kα component implies that the disk would have to be seen essentially face-on and strong relativistic effects can be ruled out. However, a face-on disk is inconsistent with previously inferred geometry.

A second weaker, but significant spectral component is present which requires either an increased optical depth in the Fe K-edge or a broad Gaussian underlying the Fe Kα line.

K. W. would like to thank A. Laor, T. Yaqoob, and H. Netzer for insightful discussions. The authors would also like to thank the referee for many helpful comments. This paper is the result of research toward the fulfillment of requirements of the Ph.D. degree at the University of Maryland.

REFERENCES

Fabian, A. C., Rees, M. J., Stella, L., & White, N. E. 1989, MNRAS, 238, 729
George, I. M., & Fabian, A. C. 1991, MNRAS, 249, 352
Halpern, J. P. 1982, Ph.D. thesis, Harvard Univ.
Holt, S. S., Mushotzky, R. F., Becker, R. H., Boldt, E. A., Serlemitsos, P. J., Szymkowiak, A. E., & White, N. E. 1980, ApJ, 241, L13
Jahoda, K. J., et al. 1993, in The International Workshop on the X-Ray Background (Spain), ed. X. Barcons & A. C. Fabian (Cambridge: Cambridge Univ. Press), 240
Kriss, G. A., et al. 1992, preprint
Kunieda, H., Turner, T. J., Awaki, H., Koyama, K., Mushotzky, R. F., & Tsusaka, Y. 1990, Nature, 345, 786
Lightman, A. P., & White, T. R. 1988, ApJ, 335, 57
Laor, A. 1991, ApJ, 376, 90
Maisack, M., & Yaqoob, T. 1991, A&A, 249, 25
Makishima, K. 1986, in The Physics of Accretion onto Compact Objects, ed. K. O. Mason, M. G. Watson, & N. E. White (Berlin: Springer), 249
Maoz, D., et al. 1991, ApJ, 367, 493
Matt, G., Perola, G. C., Piro, L., & Stella, L. 1991, A&A, 247, 25
Serlemitsos, P. J., et al. 1991, in Proc. 28th Yamada Meeting (Nagoya, Japan), Frontiers of X-ray Astronomy, ed. Y. Tanaka & K. Koyama (Tokyo: Universal Academy Press), 221
Shafer, R. A., Haberl, F., & Arnaud, K. A. 1989, XSPEC: An X-Ray Spectral Fitting Package (ESA TM-09)
Warwick, R. S., Yaqoob, T., Pounds, K. A., Matsuoka, M., & Yamauchi, M. 1989, PASJ, 41, 721
Weaver, K. A. 1993, in preparation
Yaqoob, T., & Warwick, R. S. 1991, MNRAS, 248, 773 (YW91)
Yaqoob, T., Warwick, R. S., & Pounds, K. A. 1989, MNRAS, 236, 153